LAWRENCE
LIVERMORE
NATIONAL
LABORATORY

LLNL-JRNL-481249

# The formation of metastable aluminosilicates in Al - Si - H2O system: Results from solution chemistry and solid-state NMR spectroscopy/

H. E. Mason, R. S. Maxwell, S. A. Carroll

April 26, 2011

Geochimica et Cosmochimica Acta

## Disclaimer

Available online at www.sciencedirect.com

SciVerse ScienceDirect

Geochimica et Cosmochimica Acta xxx (2011) xxx–xxx

Geochimica et Cosmochimica Acta

www.elsevier.com/locate/gca

# The formation of metastable aluminosilicates in the Al–Si–$H_2O$ system: Results from solution chemistry and solid-state NMR spectroscopy

Harris E. Mason *, Robert S. Maxwell, Susan A. Carroll

*Physical and Life Sciences Directorate, Lawrence Livermore National Laboratory, Livermore, CA 94550, United States*

Received 30 March 2011; accepted in revised form 21 July 2011

**Abstract**

We present the results of a series of experiments designed to probe the interactions between Al and the amorphous silica surface as a function of thermodynamic driving forces. The results from $^{27}Al$ single pulse magic angle spinning (SP/MAS) and $^{27}Al\{^{1}H\}$ rotational echo double resonance (REDOR) allow us to identify the reaction products and constrain their structure. In all cases, despite low Al and Si concentrations we observe the formation of metastable aluminosilicates. Results from low temperature experiments indicate that despite thermodynamic driving forces for the formation of gibbsite we observe the precipitation of separate octahedrally coordinated Al ($Al^{[6]}$) and tetrahedrally coordinated Al ($Al^{[4]}$) silicate phases. At higher temperatures the $Al^{[4]}$ silicate phase dominates the speciation. Structural models derived from the NMR data are also proposed, and the results are discussed as they relate to previous work on Al/Si cycling.
Published by Elsevier Ltd.

## 1. INTRODUCTION

Aluminum can exhibit controls on the solubility and reactivity of silica in the environment, and understanding these controls improves models of a wide range of geochemical processes such as those involved in soil chemistry, diagenesis, hydrothermal scale formation, and carbon sequestration. Measurements of biogenic silica dissolution have indicated that the solubility of silica decreases with the presence of increasing amounts of dissolved Al (Van Cappellen and Qiu, 1997a; Dixit et al., 2001; Van Cappellen et al., 2002). High pH quartz dissolution experiments have indicated that Al present even at concentrations below Al-hydroxide/oxyhydroxide saturation can significantly lower dissolution rates (Bickmore et al., 2006). The presence of dissolved Al has also been invoked to explain orders of magnitude differences between laboratory and field measured precipitation rates of hydrothermal silica scales (Gallup, 1997, 1998; Carroll et al., 1998). Identifying the controls on Al concentrations could lead to better understanding of how it affects the solubility of silica.

Thermodynamics predict that Al solubility should be controlled in most environments through the formation of aluminum hydroxides such as gibbsite or clays such as kaolinite. Metastable aluminosilicates could have important intermediary roles in the formation of these stable phases. Amorphous $Al^{[6]}$ containing aluminosilicates such as allophanes or imogolites have been identified in a variety of environments, and are common in the weathering products of volcanic ash (Parfitt, 2009). Allophane-like phases have also been implicated in controlling the bioavailability of Al (Doucet et al., 2001; Exley et al., 2002). $Al^{[4]}$ containing aluminosilicate phases have been identified as the dominant phases in hydrothermal scales (Gallup, 1997; Nishida et al., 2009) siliceous hot spring deposits (Yokoyama et al., 2004), biogenic silica (Gehlen et al., 2002), and inorganic opals (Brown et al., 2003; Paris et al., 2007). Houston et al. (2008) indicated that metastable $Al^{[4]}$ dominant aluminosilicate phases form during uptake experiments performed at pH >5 and higher dissolved silica concentrations despite thermodynamic forces driving the formation of kaolinite.

* Corresponding author. Tel.: +1 925 423 1041.
*E-mail address:* mason42@llnl.gov (H.E. Mason).

0016-7037/$ - see front matter Published by Elsevier Ltd.
doi:10.1016/j.gca.2011.07.031

Solid-state nuclear magnetic resonance spectroscopy has been applied in numerous studies to provide basic characterization of the phases formed during reactions between Al and silica. Basic differences in the Al and Si coordination environments in allophane, imogolite, and other hydrous aluminosilicates can all be identified from solid-state $^{27}$Al and $^{29}$Si NMR techniques (Barron et al., 1982; Idlefonse et al., 1994; Gallup, 1997; Exley et al., 2002; Yokoyama et al., 2002, 2004; Brown et al., 2003; Paris et al., 2007; Nishida et al., 2009). Advanced techniques which exploit the couplings between neighboring elements can provide more detailed structural determination of these Al containing phases. $^{27}$Al{$^{1}$H} cross-polarization (CP) experiments have also been applied with some success to identify the hydration state of Al in uptake experiments, but results can often be inconclusive (Stone et al., 1993; Houston et al., 2008). Rotational echo double resonance (REDOR) techniques can be used to exploit these couplings between $^{1}$H and neighboring nuclei, and have been used successfully to differentiate between different acidic sites in framework aluminosilicates (Blumenfeld et al., 1995; Blumenfeld and Fripiat, 1997). The application of more advance solid-state NMR techniques should lead to a better understanding of the types of phases which form in these systems.

The goal of this study is to investigate changes in the solid aluminosilicate speciation as a function of the thermodynamic driving forces, by varying Al concentrations, temperature, and reaction length. Low temperature flow-though experiments (25 and 50 °C) were performed at low concentrations of Al to provide optimal conditions for Al sorption or $Al(OH)_3$ precipitation. Batch experiments were conducted at 120 °C over a range of reaction lengths to explore the transitory reactions of metastable phases. Thermodynamic driving forces are estimated from the solution chemistry and structure of the Al-silicates is derived from the solid-state NMR spectroscopy.

## 2. EXPERIMENTAL METHODS

### 2.1. Flow-through experiments

Flow-through experiments were conducted at 25 and 50 °C to investigate the structure of Al at the amorphous silica surface at low concentrations (0.7–1.5 μM Al), and surface loadings using 50 ml stirred flow-through reaction vessels. About 0.25 g of high surface area amorphous silica (Mallinkrodt silica: 306 $m^2$/g surface area by BET, 75–100 μm particle size) was loaded into the reaction vessel, and reaction solutions were pumped into the constantly stirring reactor at average rates of 0.6–0.7 ml/min for periods up to 2 weeks. One set of experiments was performed with initial solution at pH 4.3 and a constant 0.7 μM Al concentration maintained throughout the experiment. During the second set, a pH 6.3 initial solution with 0.7 μM Al was reacted for several days until steady-state reaction conditions were achieved as indicated by periodic pH measurements. The 0.7 μM Al concentration represents the dissolved Al in the background electrolyte solution. After the initial equilibration step the initial Al concentration was increased to 1.5 μM. During the course of each experiment, the effluent solutions were sampled, the room temperature pH recorded, and aliquots were submitted along with initial reaction solutions for inductively coupled-plasma mass spectrometry (ICP-MS) analyses of Al and Si concentrations. At the completion of each experiment, the solids were separated and washed with distilled and deionized water via suction filtration, and placed in a 60 °C oven overnight to dry.

### 2.2. High temperature batch experiments

The transformation of the Al structure on amorphous silica was investigated at 120 °C in batch experiments. Prior to the addition of the amorphous silica solid, 60 ml of 0.5 mM Al reaction solutions were prepared with a 0.1 M NaCl background electrolyte in PTFE lined Parr acid digestion vessels. The starting solutions were adjusted to a pH of 3 and 9 using 0.1 N HCl and 1.0 N NaOH, respectively. A 10 ml aliquot of the initial solution was removed, passed through a 0.2 μm filter, and analyzed by ICP-MS to measure the initial starting solution composition. Then 0.25 g amounts of the same amorphous silica used in flow-through experiments were added to the solutions, the vessels sealed immediately and placed into a 120 °C oven for up to 15 days. After a set reaction time, the vessels were removed from the oven and allowed to cool for 1 h before collection of the final samples. Aqueous samples were filtered and acidified with high purity $HNO_3$ and stored at room temperature prior to chemical analysis. The final pH values of these solutions were also recorded after the solutions had cooled to room temperature. The solids were separated and washed with distilled and deionized water via suction filtration, and placed in a 60 °C oven overnight to dry.

### 2.3. Model minerals

Minerals were used to compare their NMR spectral features to those of the uptake samples. The hydrated zeolite phases analcime, mordenite, clinoptilolite-Na were used as standards for $Al^{[4]}$ in association with structural water molecules. Kaolinite and gibbsite were used as model minerals containing $Al^{[6]}$ only in association with structural hydroxyl. Additionally, a sample of beidellite was used as a standard where both $Al^{[6]}$ and $Al^{[4]}$ coordination environments are present. The sources and general chemical formulae for the model mineral are presented in Table 1.

### 2.4. Solid-state NMR spectroscopy

$^{27}$Al single pulse magic angle spinning (SP/MAS), $^{27}$Al{$^{1}$H} rotational echo double resonance (REDOR), and $^{23}$Na SP/MAS NMR spectra were all collected on a Bruker Avance 400 spectrometer (9.4 T) at operating frequencies of 400.09, 104.25, and 105.83 MHz for $^{1}$H, $^{27}$Al, and $^{23}$Na, respectively. Samples were contained in 4 mm (o.d.) $ZrO_2$ rotors, and spectra were collected using a Bruker 4 mm triple resonance solids probe. $^{27}$Al SP/MAS spectra were collected at a 10 kHz spinning rate using a selective 1 μs excitation pulse (solution $\pi/2 = 14.5$ μs) and a 0.2 s recycle delay for 10,000 to 900,000 acquisitions. The short

Please cite this article in press as: Mason H. E., et al. The formation of metastable aluminosilicates in the Al–Si–$H_2O$ system: Results from solution chemistry and solid-state NMR spectroscopy. *Geochim. Cosmochim. Acta* (2011), doi:10.1016/j.gca.2011.07.031

Table 1
Mineral samples used for comparison of NMR properties.

| Mineral | General chemical formula | Location | Source |
|---|---|---|---|
| Analcime | $Na_2Al_2Si_4O_{12}{\cdot}2H_2O$ | Barstow, CA, USA | Mineral Research, Clarkson NY |
| Clinoptilolite | $(Na,Ca,K)_{2-3}Al_3(Al,Si)_2Si_{13}O_{36}{\cdot}12H_2O$ | Castle Creek, ID, USA | Mineral Research, Clarkson NY |
| Mordenite | $Na_2Al_2Si_{10}O_{24}{\cdot}7H_2O$ | India | |
| Kaolinite; KGa-1b | $Al_2Si_2O_5(OH)_4$ | Washington Co., GA, USA | Clay Mineral Society |
| Gibbsite | $Al(OH)_3$ | Synthetic | |
| Beidellite SBId-1 | $(Na,Ca_{0.5})_{0.3}Al_2(Al,Si)_4O_{10}(OH)_2{\cdot}nH_2O$ | ID, USA | Clay Mineral Society |

0.2 s pulse delay was chosen to optimize signal acquisition, but spectra taken at a 5 s pulse delay of select samples (not shown) indicated no differences in the relative peak abundances indicating that spectra collected at short pulse delays sufficiently represent the distribution of the Al species. $^{27}$Al SP/MAS NMR was also run on rotor blanks and no background signal was observed after 2 days of acquisition time. $^{27}$Al multiple quantum (MQ) MAS spectra were collected at a spinning rate of 13 kHz using 3 μs excitation and 1 μs conversion pulses, followed by a 28 μs *z*-filter pulse. A total of 32 points were collected with an increment of 38.5 μs in *t*1 corresponding to a spectral window of 26 kHz in the isotropic dimension. Forward linear prediction procedures were used to complete the signal in *t*1 to avoid truncation errors. The $^{27}$Al MQ/MAS data were processed using standard shearing methods. $^{27}$Al{$^1$H} REDOR were collected with a 10 kHz spinning rate at a variety of dephasing periods using spin–echo pulses for $^{27}$Al ($\pi = 8$ μs), and 10 μs recoupling pulses for $^1$H. $^{23}$Na SP/MAS NMR spectra were also collected at 10 kHz spinning rate using a short, selective 1 μs pulse (solution $\pi/2 = 18$ μs) and a 0.5 s recycle delay. Additional $^{23}$Na SP/MAS NMR spectra were collected at a higher magnetic field strength of 11.7 T on a Bruker AMX 500 spectrometer using a 4 mm Bruker broadband X double resonance probe with a spinning rate of 3 kHz, a 1 μs pulse (solution $\pi/2 = 18$ μs), and a 0.5 s pulse delay. $^{29}$Si{$^1$H} cross-polarization (CP) MAS NMR spectra were collected on a Tecmag Apollo 300 spectrometer at operating frequencies of 300.19 and 59.63 MHz for $^1$H and $^{29}$Si, respectively. Samples were contained in 7.5 mm (o.d.) $ZrO_2$ rotors, and spectra were collected at 3 kHz with a 2 ms CP contact time using a 7.5 mm Chemagnetics probe. $^{27}$Al and $^{23}$Na spectra were referenced to external solution standards of 0.1 M $AlCl_3$ ($\delta_{Al} = 0.0$ ppm) and 0.1 M NaCl ($\delta_{Na} = 0.0$ ppm), respectively. $^{29}$Si spectra were referenced with respect to tetramethyl silane using solid kaolinite as an external shift reference ($\delta_{Si} = -92.0$ ppm; Magi et al., 1984). The NMR spectra were also subjected to least squares fitting to a linear combination of pseudo-Voight lineshapes in order to extract their peak positions and integrated intensities. Peaks showing large asymmetries required multiple peaks to provide adequate fits. Spectral intensities of spectra used in REDOR analysis were obtained using self consistent models where the only the intensities were allowed to vary while all other spectral parameters were fixed.

We advocate the use of the $^{27}$Al{$^1$H} REDOR experiment over the more commonly used $^{27}$Al{$^1$H} CP/MAS experiment to examine the connectivity of Al and H in geochemical systems for a variety of reasons. When the target nucleus is a quadrupole like $^{27}$Al a decrease in the signal intensity compared to SP/MAS spectra is generally observed. This signal loss leads to an increase in the experimental time needed to collect a useful spectrum. In addition, CP between $^1$H and quadrupolar nuclei is highly sensitive to sample spinning rate, radio frequency strength, and the magnitude of the quadrupolar coupling constant (Vega, 1992). One must undertake careful experimental setup on the sample of interest in order to derive useful, quantitative data. In geochemical systems where low signal intensities could be expected, the standard procedure is to use a model compound such as gibbsite as a setup standard, but this procedure is flawed since we cannot assume the quadrupole coupling constants of our unknown samples are the same as that for gibbsite. We can gain more accurate information using the $^{27}$Al{$^1$H} REDOR experiment which takes little additional setup beyond that undertaken for SP/MAS experiments, and can be setup using model compounds since it relies only on the dipole coupling between $^{27}$Al and $^1$H without any dependencies upon $^{27}$Al quadrupolar coupling.

The REDOR experimental procedure includes the collection of two separate $^{27}$Al spectra. The first spectrum is produced by collecting a standard $^{27}$Al spin–echo experiment ($S_0$) which, like the $^{27}$Al SP/MAS experiment, contains peaks from all the $^{27}$Al species present in the sample. The second spectrum, the REDOR spectrum ($S$), is produced by introducing $^1$H pulses which recouple the $^{27}$Al–$^1$H dipolar coupling, and will contain peaks of reduced intensity for any species associated with $^1$H. Subtraction of the two spectra produces a difference spectrum ($\Delta S$) which only has peaks from $^{27}$Al species in close spatial proximity to $^1$H (<5 Å). This experiment is synchronized with the sample spinning, and the total duration of the experiment is called the REDOR dephasing period. A REDOR dephasing curve can be constructed by plotting the REDOR fraction ($\Delta S/S_0$) as a function of the REDOR dephasing period. The shape of this curve depends upon the local Al–H configuration, and can be used to draw interpretations about local structure. It is important to recognize that these effects only occur if the $^{27}$Al species is associated with rigidly bound $^1$H. A review of the REDOR technique can be found in Gullion and Vega (2005).

### 2.5. ICP-MS solution analyses

The ICP-MS analyses of the reaction solutions were performed on a Thermo Electron X Series quadrupole

Please cite this article in press as: Mason H. E., et al. The formation of metastable aluminosilicates in the Al–Si–$H_2O$ system: Results from solution chemistry and solid-state NMR spectroscopy. *Geochim. Cosmochim. Acta* (2011), doi:10.1016/j.gca.2011.07.031

ICP-MS. A fully quantitative analysis using a linear calibration curve based on known standards was performed. The internal standard corrected for instrument drift and suppression from the sample matrix. Si was run in CCT (Collision Cell Technology) mode due to polyatomic interferences. Samples were run with either a 10× or 100× dilution to ensure analytes fell within the calibration range. These results were corrected back through the 10× or 100× dilution and reported as molar concentrations. NIST traceable certified reference materials and serial dilutions are analyzed for accuracy. For an estimate of precision, at least one sample is run in duplicate per batch.

### 2.6. Geochemical modeling

Thermodynamic conditions of the experiments were estimated using equilibrium geochemical speciation and solubility modeling using the Geochemists Workbench v8.0 (Betke and Yeakel, 2010). We used the standard thermo.dat database for all calculations. Al activity versus pH diagrams were calculated at a fixed Si concentration derived from average measured solution compositions. The selected minerals albite, pyrophyllite, and paragonite were suppressed during construction of the activity diagrams since their formation is assumed to be kinetically hindered in our experiments. The reaction pH values for the 50 and 120 °C experiments were extrapolated by running equilibrium calculations where the final solution compositions were first equilibrated at 25 °C and pH and then reacted to the final reaction temperature. The precipitation of all minerals was suppressed during the pH calculations assuring that solution compositions remained constant and only pH was allowed to fluctuate.

## 3. RESULTS

### 3.1. Thermodynamic landscape

Equilibrium phase diagrams for the Al–Si–$H_2O$ system were constructed from the measured solution chemistry for the 25, 50 and 120 °C experiments (Fig. 1 and Tables 2 and 3). Thermodynamic analysis of the steady-state solution compositions at 25 and 50 °C indicate that in all cases gibbsite is the predicted stable phase which contains only $Al^{[6]}$ (Fig. 1a and b). Additionally, all low temperature experiment solutions were undersaturated with respect to amorphous silica. At pH 6.3 the time resolved solution data show a drop in the Si concentration that corresponds with the addition of Al to the reaction solutions (Fig. 2). This decrease in the Si effluent concentration is consistent with the results of Houston et al. (2008) indicating the precipitation of an aluminosilicate phase. The pH, Al, and Si concentrations remain relatively constant throughout the remainder of the experiments and indicate that steady-state reaction conditions have been achieved. The low degree of scatter present in these data also indicates that there is no significant contribution to the solution chemistry from the presence of colloidal particles which are also consistent with the results of Houston et al. (2008).

Thermodynamic analyses of the solution compositions at 120 °C predict differing phase stability for pH 2.9 and 5.9 samples. The pH of these samples changes significantly from their initial values due to the reaction at temperature. We will refer to these experiments generically as the low pH and near-neutral pH experiments in all future discussion. At low pH the final solution compositions plot within the kaolinite ($Al^{[6]}$ only) stability field. Contrastingly, the final solution compositions of the high pH samples place them firmly within the mordenite-Na ($Al^{[4]}$ only) stability field (Fig. 1c). These data predict that at low pH conditions $Al^{[6]}$ species should dominate, but at near-neutral pH conditions $Al^{[4]}$ phases should dominate. Again in all cases, these solutions are undersaturated with respect to amorphous silica. Despite using the same stock solution for all experiments, the solution analyses indicates a lower initial Al concentration for the higher pH samples which likely result from immediate precipitation of small amounts of Al oxides/oxyhydroxides. We observe no significant trends in the solution chemistry with time. Nearly all Al is removed from solution during these experiments and consumption increases only slightly with increased sample aging indicating the reaction of Al with the silica surface is mostly complete after 3 days.

### 3.2. Al coordination environment in the precipitates

Solid-state $^{27}Al$ SP/MAS NMR spectra obtained for 25, 50 and 120 °C samples are presented in Figs. 3 and 4. The positions of the peak maxima and relative peak intensities for all samples are presented in Table 4. The asymmetric shape of the peaks likely results from a combined distribution of chemical shifts and quadrupole coupling constants characteristic of disordered phases. Most samples show mixed coordination with peaks centered at 0–10 ppm assigned to Al in sixfold coordination, and those centered at 43–56 ppm assigned to Al in fourfold coordination. Peaks representing Al in fivefold coordination ($Al^{[5]}$) in the 20–40 ppm range were not observed as discrete peaks in the SP/MAS spectra. Any overlap of the $Al^{[6]}$ and $Al^{[4]}$ peaks, and the low signal to noise in some samples could easily mask $Al^{[5]}$ peaks, if present.

At 25 °C the relative intensity of four- and six-coordinated Al is similar at pH 6.3 and 4.3 indicating that Al retains the same structural environment as the surface loading increased from pH 4.3 to 6.3 (Fig. 3a and b). The peak positions and relative intensities are well within the experimental uncertainty due to the spectral noise in the pH 4.3 spectrum (Fig. 3b). The spectra of 50 °C samples (Fig. 3c–e) produce peaks centered at about the same chemical shift as the 25 °C sample, but with drastically different relative intensities. In the pH 4.3 experiment, a significant amount of amorphous silica adhered to the reactor vessel walls, and was collected and analyzed as a separate sample from the bulk. The spectrum collected of the bulk shows the $Al^{[6]}$ peak dominating over the $Al^{[4]}$ peak (Fig. 3d). The relative intensity of four- and six-coordinated Al in the wall adhered sample (Fig. 3e) is similar to the 25 °C data (Fig. 3b). At pH 6.3 no silica was observed adhered to the reactor walls and therefore only the bulk sample was

Please cite this article in press as: Mason H. E., et al. The formation of metastable aluminosilicates in the Al–Si–$H_2O$ system: Results from solution chemistry and solid-state NMR spectroscopy. *Geochim. Cosmochim. Acta* (2011), doi:10.1016/j.gca.2011.07.031

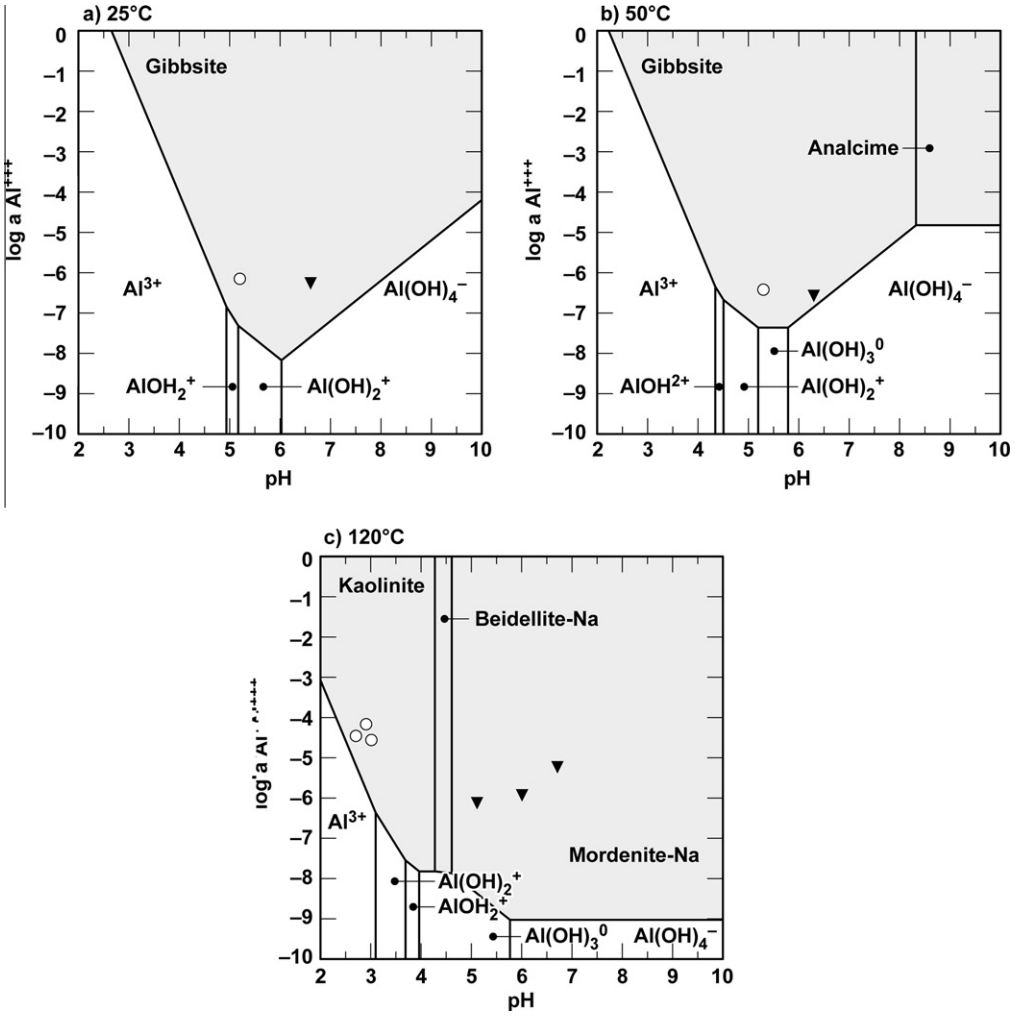


Fig. 1. Equilibrium phase diagrams for the Al–H system constructed from the measured solution chemistry. In addition to the Al the systems are in equilibrium with 0.1 M NaCl and Si equivalent to the average measured Si concentration measured from experiments conducted at the same temperature (see Tables 1 and 2). The solid points represent measured Al concentrations and pH conditions for the respective experiments. (a and b) The points represent average values when steady-state conditions were achieved. Solid circles represent data from the low Al concentration experiments and solid triangles represent that from high concentration experiments. (c) Points here represent the final pH and Al concentrations of the low pH experiments (solid circles) and high pH experiments (solid triangles).

Table 2
Results of solution chemistry analyses for flow-through experiments. Steady-state values are given as the average value. The final steady-state pH values for the 50 °C experiments were calculated at temperature using the measured room temperature pH shown in parentheses. Initial Si concentrations for the pH 6.3 experiments are the steady-state concentrations before the addition of Al to the solution. Si concentrations in the pH 4.3 experiments remained at the steady-state [Si] during the entire experiment.

| Sample ID | Temp. (°C) | Initial pH | Initial [Al] added (μM) | Steady-state pH | Steady-state [Al] (μM) | Steady-state [Si] (μM) |
|---|---|---|---|---|---|---|
| FTRT pH 4 | 22 | 4.4 | 0.7 | 5.2 | 0.7 | 13.1 |
| FTRT pH 6 | 22 | 6.3 | 1.6 | 6.6 | 0.6 | 7.4 |
| FT50 pH 4 | 50 | 4.3 | 0.7 | 5.3 (5.4) | 0.4 | 120.9 |
| FT50 pH 6 | 50 | 6.3 | 1.4 | 6.3 (6.5) | 0.3 | 196.5 |

analyzed. The collected spectrum shows the $Al^{[6]}$ peak is dwarfed by the dominant $Al^{[4]}$ peak (Fig. 3c). The NMR results presented here align with those presented by Houston et al. (2008) where $Al^{[4]}$ peaks dominate in uptake samples produced over a wide range of pH conditions, but are in stark contrast to the predictions of the solution chemistry.

As temperature increases, $Al^{[4]}$ coordination dominates as is shown by spectra collected from the 120 °C experiments (Fig. 4). Only minor peaks from $Al^{[6]}$ are present representing a minor fraction of the total spectral intensity observed (<2%). These peaks are likely residual Al-oxides/hydroxides that formed prior to the addition of the

Table 3
Results of solution chemistry analyses for high temperature batch experiments. All samples were synthesized at a temperature of 120 °C. The final pH values were calculated at temperature using the measured room temperature pH shown in parentheses. In all cases initial [Si] was below the detection limit of the ICP-MS method.

| Sample ID | Aging (days) | Initial pH | Initial [Al] added (μM) | Final pH | Final [Al] (μM) | Final [Si] (μM) |
|---|---|---|---|---|---|---|
| HT LpH 3d | 3 | 4.3 | 481 | 2.9 (2.9) | 66.7 | 6293 |
| HT LpH 7d | 7 | 4.3 | 483 | 2.7 (2.7) | 34.3 | 6912 |
| HT LpH 15d | 15 | 4.3 | 490 | 3.0 (3.0) | 26.6 | 6856 |
| HT LpH 3d | 3 | 9.0 | 153 | 6.7 (7.4) | 6.4 | 5014 |
| HT LpH 8d | 8 | 8.8 | 133 | 6.0 (6.6) | 1.3 | 4743 |
| HT LpH 14d | 14 | 8.0 | 50.3 | 5.1 (5.3) | 0.8 | 6560 |

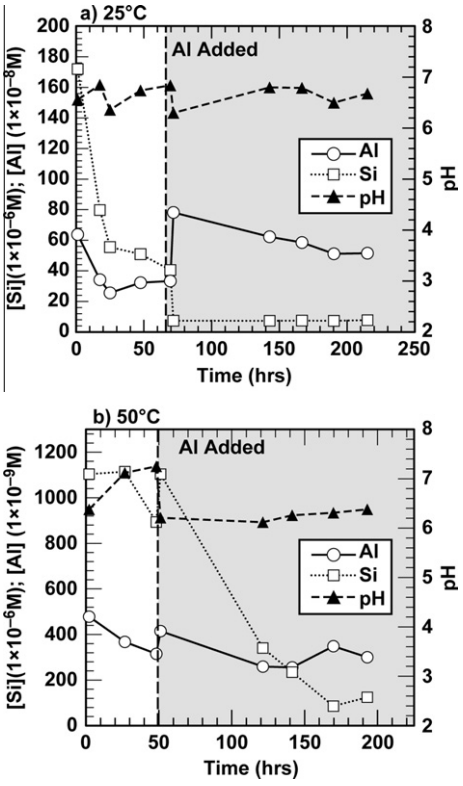


Fig. 2. Effluent solution chemistry data for the (a) 25 °C and (b) 50 °C pH 6.3 experiments as a function of time. Open symbols represent Al (diamonds) and Si (squares) solution concentrations derived from ICP-MS. Closed triangles represent measured pH values. Dotted lines are provided to guide the eye. A dashed vertical line has also been placed at the time when Al was added to the reaction solution.

amorphous silica to the Al starting solution. Given their low intensity it is likely the phases dissolve back into solution during the reaction at temperature. No significant changes in the peak positions or relative intensities are observed with increased reaction times. We can state that, aside from the pH 4.3 bulk sample at 50 °C, in all sets of low and high temperature samples the Al speciation is dominated by the presence of four-coordinate Al phase since care was taken to collect these spectra under quantitative conditions (i.e. using short selective excitation pulses).

Additionally, $^{27}$Al MQ/MAS spectra were collected for two samples, the 25 °C pH 6.3 and 120 °C 15 day low pH samples, in order to accurately determine the $^{27}$Al isotropic chemical shifts ($\delta_{iso}$) and quadrupole coupling constants ($C_{qcc}$). A representative contour plot for the 25 °C pH 6.3 sample is presented in Fig. 5. For the $Al^{[6]}$ peak in the 25 °C sample, we obtain a $\delta_{iso}$ of 10.5 ppm with an average $C_{qcc}$ of 18.7 MHz. For the $Al^{[4]}$ peaks in the low and high temperature samples, we obtain $\delta_{iso} = 60.2$ ppm, $C_{qcc} = 6.1$ MHz and $\delta_{iso} = 54.6$ ppm, $C_{qcc} = 5.3$ MHz, respectively. The isotropic chemical shift for the $Al^{[6]}$ peak shows much greater variability from the peak maxima than those for the $Al^{[4]}$ peaks indicating that the peak maxima is a poor comparison for the $Al^{[6]}$ peaks, but is comparable for the $Al^{[4]}$ peaks. In the spectral sets for both samples, we see a smearing of the contours along the $C_{qcc}$ axis (blue line in Fig. 5) for all peaks which is characteristic of a distribution of the quadrupole coupling constants, but only small distributions along the chemical shift axis (red line in Fig. 5). This indicates that the asymmetric lineshapes observed in the $^{27}$Al SP/MAS spectra result from distributions in $C_{qcc}$ with smaller influence from distributions in chemical shift. In addition, no peaks are observed in these spectra attributable to the presence of $Al^{[5]}$ in these samples.

Additional information about the identity of the Al in these samples can be gained from analysis of their $^{29}$Si{$^{1}$H} CP/MAS NMR spectra. Characteristic spectra collected for these samples are presented in Fig. 6. The majority of the spectra show the same three peaks at −94, −101 and −112 ppm which are characteristic of $Q^2$, $Q^3$, and $Q^4$ silica sites in amorphous silica. There are minor changes in the relative intensity of these peaks, but these can be easily attributed to pH effects on the silica surface speciation (Carroll et al., 2002). These results suggest that for the majority of the samples the main silica speciation does not change substantially from amorphous silica. We, however, observe a peak at −79.3 ppm in the spectrum collected for the 50 °C pH 4.3 bulk sample (Fig. 5b) which is characteristic of the aluminosilicate phases imogolite, $Al_2SiO_3(OH)_4$, and allophane, $xAl_2O_3{\cdot}ySiO_2{\cdot}zH_2O$ (Barron et al., 1982; Idlefonse et al., 1994). We collectively refer to the phase as allophane, because imogolite and allophane can exhibit similar NMR spectral features (Idlefonse et al., 1994). Chemical analyses would be needed to differentiate between imogolite and various types of allophanes. The allophane peak is weak compared to the other peaks present in the CP spectrum from the amorphous silica, and is absent from the $^{29}$Si SP/MAS NMR spectrum (not shown) indicating that it represents a minor amount of the total Si speciation in this sample. It is entirely absent

Please cite this article in press as: Mason H. E., et al. The formation of metastable aluminosilicates in the Al–Si–$H_2O$ system: Results from solution chemistry and solid-state NMR spectroscopy. *Geochim. Cosmochim. Acta* (2011), doi:10.1016/j.gca.2011.07.031

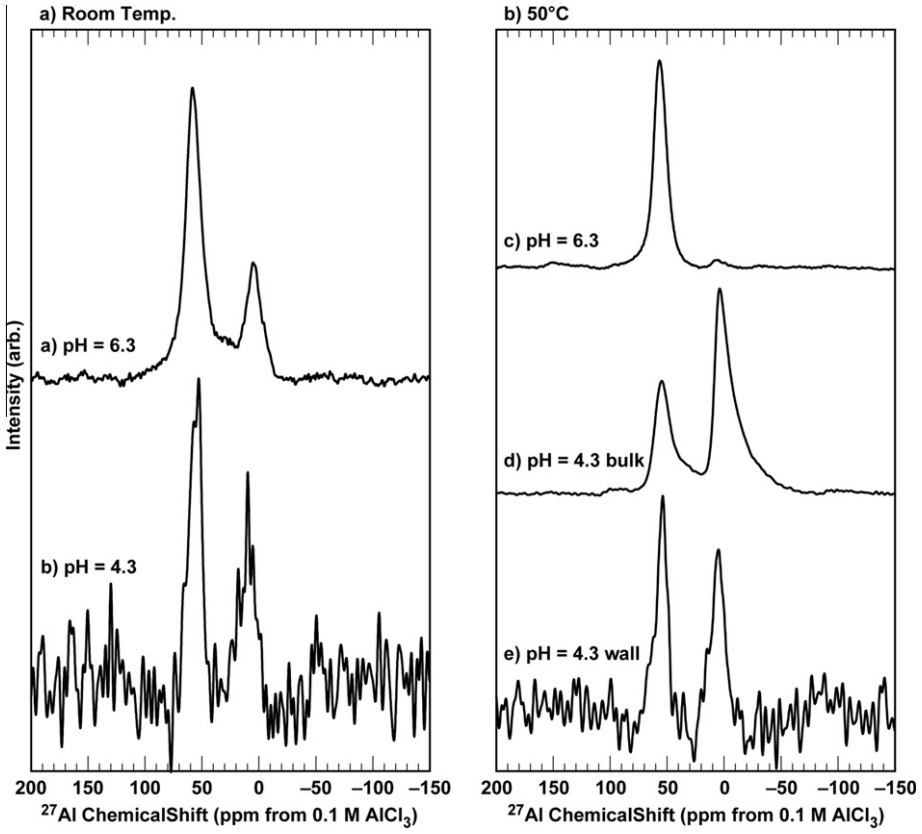


Fig. 3. $^{27}$Al SP/MAS NMR spectral sets collected for samples obtained from (left) 25 °C and (right) 50 °C experiments.

in the $^{29}$Si spectra collected for the other samples. If this phase or other aluminosilicates are present in the other samples, the representative peaks are masked by the majority peaks. It is possible, therefore, that $^{27}$Al spectral characteristics could be used as tracers for the presence of allophane phases. Allophane contains only Al$^{[6]}$ and since the $^{27}$Al spectrum of the 50 °C sample produced at pH 4.3 contains substantial amounts of Al$^{[6]}$ we attribute its presence to allophane-like phases (cf. Fig. 3d).

### 3.3. Hydration state of the Al phases

Many possible Al containing phases could be present in these systems that could produce similar $^{27}$Al spectra. Exploiting the differences in their hydration state using $^{27}$Al{$^{1}$H} REDOR is a potential method to differentiate among these phases. A representative $^{27}$Al{$^{1}$H} REDOR spectral set for the 25 °C pH 6.3 sample is presented in Fig. 7. We collected data for the 25 °C sample produced at pH 6.3, both the 50 °C sample made at pH 4.3 and 6.3, and the 120 °C samples at low pH (3 and 7 days) and near-neutral pH (14 days) to span the largest range of solution conditions using the fewest number of samples. These experiments are time-consuming due to the low Al concentrations present, and it is impractical to collect REDOR spectral sets for every sample.

In all cases, we observe the presence of the same peaks in the difference spectra as in the echo spectra indicating that all the $^{27}$Al peaks present are coupled to $^{1}$H. The REDOR fractions observed at 1.2 ms dephasing period for the studied samples are summarized in Table 5. We note the highest REDOR fractions for the 25 °C pH 6.3 and 50 °C pH 4.3 bulk samples with higher fractions for Al$^{[6]}$ than Al$^{[4]}$. However, we still observe substantial REDOR fractions for all the Al$^{[4]}$ peaks in the other investigated samples. These robust REDOR fractions for the Al$^{[4]}$ peaks indicate a strong association with hydrated species. This contrasts previous results from $^{27}$Al{$^{1}$H} cross-polarization (CP) MAS experiments which show little association of Al$^{[4]}$ with $^{1}$H (Stone et al., 1993; Houston et al., 2008).

Comparison of the REDOR fraction versus dephasing period of the unknowns to model systems allows us to elucidate the structure of Al in our study. Characteristic REDOR curves produced for model minerals and the corresponding data points for the uptake experiments are presented for in Fig. 8. The Al$^{[6]}$ minerals all produce reasonably strong dephasing behavior following the same general trend with gibbsite producing the highest REDOR fractions, followed by kaolinite, and the Al$^{[6]}$ peak of beidellite (Fig. 8a). This result aligns well with the relative Al:H ratios of the Al$^{[6]}$ peak which, respectively, are 1:3, 1:2, and 1:1 for gibbsite, kaolinite, and beidellite. This indicates the magnitude of the REDOR fraction is a greater tracer for the hydration state than the overall trend. For the Al$^{[4]}$ containing minerals, analcime and beidellite produce the highest REDOR fractions (Fig. 8b). Despite containing

Please cite this article in press as: Mason H. E., et al. The formation of metastable aluminosilicates in the Al–Si–$H_2O$ system: Results from solution chemistry and solid-state NMR spectroscopy. *Geochim. Cosmochim. Acta* (2011), doi:10.1016/j.gca.2011.07.031

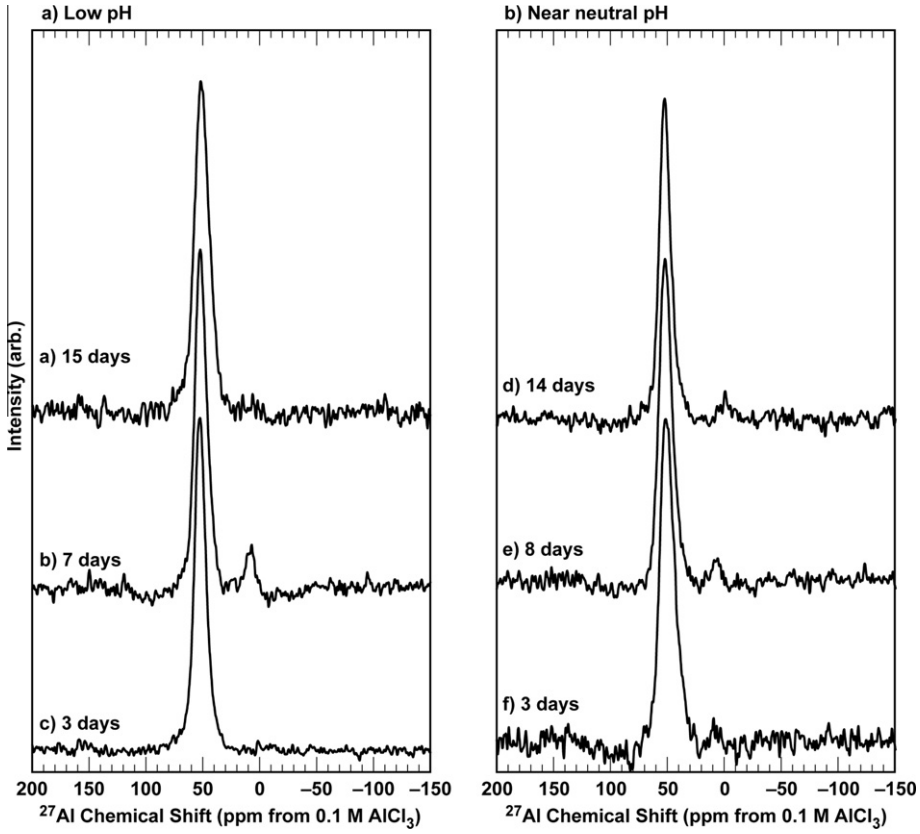


Fig. 4. $^{27}$Al SP/MAS NMR spectral sets collected for samples obtained from (left) low pH and (right) high pH 120 °C experiments.

Table 4
$^{27}$Al and $^{23}$Na NMR spectral parameters. $^{27}$Al isotropic chemical shift determined from MQ/MAS are presented for selected samples in parentheses. $^{27}$Al intensities are given as the relative fraction of the total spectral intensity. Intensities not given for $^{23}$Na.

| Sample ID | $^{27}$Al (ppm) | | Relative intensity | | $^{23}$Na (ppm) |
|---|---|---|---|---|---|
| | 6 CN | 4 CN | 6 CN | 4 CN | |
| FTRT pH 4 | 9.8 | 55.7 | .38 | .62 | n.m. |
| FTRT pH 6 | 5.2 (10.5) | 57.8 (62.3) | .26 | .74 | −8.1 |
| FT50 pH 4 wall | 5.3 | 54.5 | .47 | .53 | n.m. |
| FT50 pH 4 bulk | 4.7 | 54.8 | .62 | .38 | n.m. |
| FT50 pH 6 | 5.0 | 56.1 | .02 | .98 | −5.6 |
| HT LpH 3d | N/A | 52.3 | – | 1.0 | −5.9 |
| HT LpH 7d | 8.3 | 51.8 | .07 | .93 | −5.7 |
| HT LpH 15d | N/A | 50.9 (54.6) | – | 1.0 | −4.9 |
| HT NpH 3d | N/A | 50.5 | – | 1.0 | −7.7 |
| HT NpH 8d | 7.2 | 51.8 | .03 | .96 | −9.6[a] |
| HT NpH 14d | −0.9 | 52.4 | .05 | .95 | −5.2 |

[a] Spectrum also contains sharp peak at 7.3 ppm from solid NaCl n.m. spectrum not measured.

substantial $H_2O$ in its chemical formula mordenite produces a relatively weak dephasing curve. Clinoptilolite was also investigated (not shown), but did not exhibit an appreciable REDOR effect at any of the dephasing periods investigated despite its $H_2O$ content. Unlike the Al$^{[6]}$ phases, the magnitude of the REDOR fraction for Al$^{[4]}$ phases does not correlate to the Al:H ratio as evidenced by the 1:1 ratio for analcime, and the 1:7 ratio for mordenite. In the Al$^{[6]}$ phases, the $^1$H is present as rigid structural hydroxyl groups and robust dephasing is expected. The $^1$H in the Al$^{[4]}$ phases is present as water molecules which are more likely to be mobile, and the differences amongst phases are likely attributable to the relative mobility of water. In the analcime structure water is motionally confined which leads to strong dipole coupling between $^{27}$Al and $^1$H corresponding to high REDOR fractions, but in

Please cite this article in press as: Mason H. E., et al. The formation of metastable aluminosilicates in the Al–Si–$H_2O$ system: Results from solution chemistry and solid-state NMR spectroscopy. *Geochim. Cosmochim. Acta* (2011), doi:10.1016/j.gca.2011.07.031

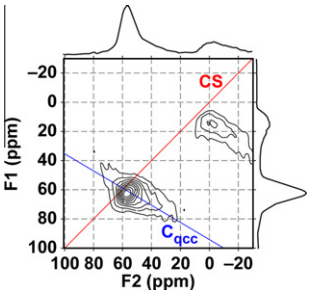


Fig. 5. 2D $^{27}$Al MQ/MAS NMR spectrum of the 25 °C pH 6.3 sample. F1 is the isotropic dimension and F2 is the MAS dimension. Red line marks the 1:1 chemical shift axis, and the blue line marks the quadrupolar axis. (For interpretation of the references to color in this figure legend, the reader is referred to the web version of this article.)

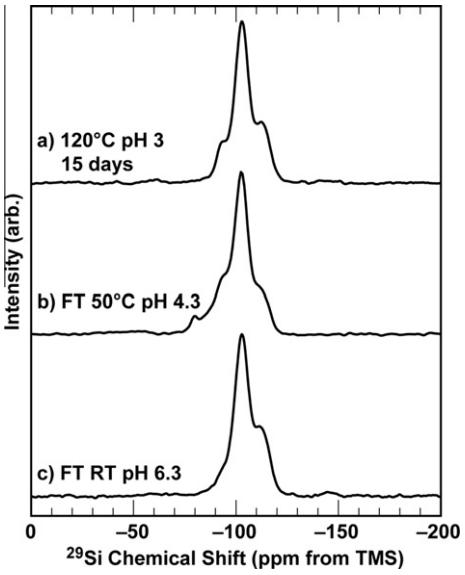


Fig. 6. Representative $^{29}$Si{$^{1}$H} CP/MAS spectra collected for the (a) low pH 120 °C sample reacted for 15 days, (b) the 50 °C sample made at pH 4.3, and (c) 25 °C sample made at pH 6.3.

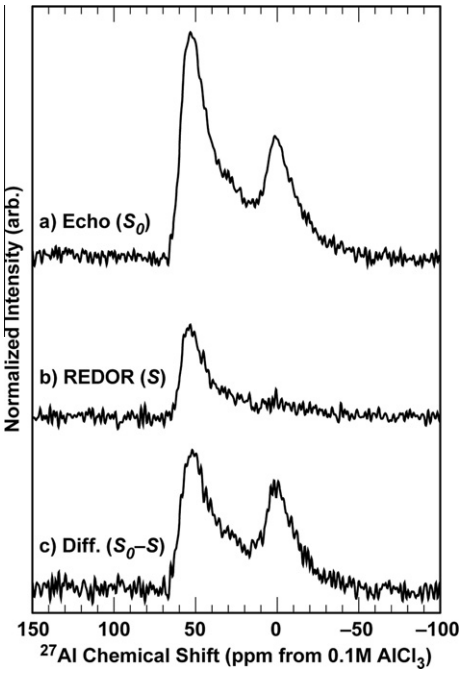


Fig. 7. Typical $^{27}$Al{$^{1}$H} REDOR spectral set collected for the 25 °C pH 6.3 sample at a dephasing period of 1.2 ms. (a) $^{27}$Al spin–echo control spectrum, (b) $^{27}$Al{$^{1}$H} REDOR spectrum. (c) Difference spectrum obtained from subtraction of (a) and (b).

Table 5
$^{27}$Al{$^{1}$H} REDOR fractions measured for Al$^{[6]}$ and Al$^{[4]}$ peaks at 1.2 ms dephasing time for selected samples.

| Sample ID | REDOR fraction $(S_0 - S)/S_0$ | |
|---|---|---|
| | 6 CN | 4 CN |
| FTRT pH 6 | 0.83 | 0.62 |
| FT50 pH 4 bulk | 0.90 | 0.64 |
| FT50 pH 6 | – | 0.45 |
| HT LpH 3d | – | 0.42 |
| HT LpH 7d | – | 0.45 |
| HT NpH 14d | – | 0.43 |

mordenite the more open structure allows more freedom of motion which reduces the coupling between $^{27}$Al and nearby $^{1}$H (Alberti et al., 1986; Moroz et al., 1998).

The REDOR fractions for the Al$^{[6]}$ peak in the 25 °C pH 6.3 and 50 °C pH 4 experiments trends closely with the dephasing curve produced for kaolinite (Fig. 8a). Peaks for Al$^{[6]}$ are observed for the other samples subjected to REDOR analysis, but their intensities were too low to derive accurate measures of their dephasing. The majority of samples studied exhibit dephasing behavior for Al$^{[4]}$ mimicking that of analcime (Fig. 8b). The exception to this trend are the Al$^{[4]}$ peaks in the 25 °C pH 6.3 and 50 °C pH 4.3 samples which produce higher REDOR fractions.

### 3.4. The role of Na in structural balancing Al uptake

The existence of Al$^{[4]}$ in association with silica in these samples is unlikely without the presence of additional charge and structural balancing components. In our systems, this role could be filled by the $Na^+$ cation. Therefore, we collected $^{23}$Na SP/MAS NMR spectra of these samples to investigate the local structure of Na present in these samples (Fig. 9). With one exception, all spectra collected at 9.4 T contain a single broad asymmetric $^{23}$Na peak. The exception is the near-neutral pH 120 °C sample collected at 8 days which shows an additional sharp peak at 7.3 ppm which arises from residual crystalline NaCl from drying the sample. A survey of the 9.4 T $^{23}$Na NMR data presented in Table 4 reveals that the position of the peak maxima in all these samples falls within a chemical shift range of −4.9 to −9.8 ppm. Contrastingly, the spectra collected at 11.7 T for selected samples exhibit a sharper peak centered near −1 ppm, but are underlain by a broad, poorly defined signal which is difficult to accurately deconvolute from the main peak. These spectra are similar to those

Please cite this article in press as: Mason H. E., et al. The formation of metastable aluminosilicates in the Al–Si–$H_2O$ system: Results from solution chemistry and solid-state NMR spectroscopy. *Geochim. Cosmochim. Acta* (2011), doi:10.1016/j.gca.2011.07.031

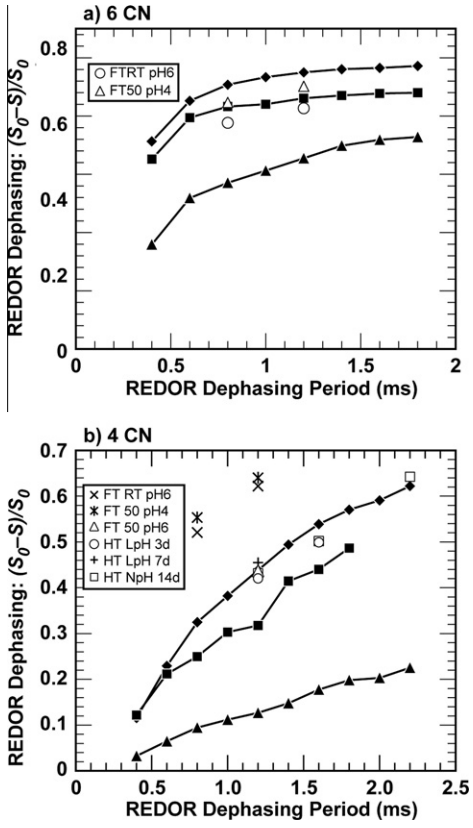


Fig. 8. $^{27}Al\{^{1}H\}$ REDOR fraction as a function of dephasing period. (a) $Al^{[6]}$ containing minerals gibbsite (♦), kaolinite (■), and beidellite (▼) and the $Al^{[6]}$ peaks for studied samples (open symbols). (b) $Al^{[4]}$ containing minerals analcime (♦), beidellite (■), and mordenite (▼) and the $Al^{[4]}$ peaks for studied samples (open symbols). The dashed lines are provided for the minerals to guide the eye. Sample IDs correspond to those presented in Table 3.

observed for sorbed Na on the surface of silica where the peak maxima generally occur in the region of 0 to −3.0 ppm (Kim and Kirkpatrick, 1997; Carroll et al., 2002). Therefore, the majority of the observed signal likely represents Na cations sorbed to the silica surface. However, the breadth of the spectra collected at both fields cover the range reported for $^{23}Na$ NMR peaks for the aluminosilicates albite (Xue and Stebbins, 1993) and analcime (Kim and Kirkpatrick, 1998), and such broad peaks could easily mask additional Na containing phases present at minor amounts.

## 4. DISCUSSION

### 4.1. Structure of the solid precipitates

Using the results of the NMR study we can begin to determine the possible nature of the Al species present beyond the simple assignment to $Al^{[6]}$ and $Al^{[4]}$ species. Since we observe peaks for $Al^{[4]}$ in the range of 51–59 ppm, we assign these peaks to $AlO_4$ tetrahedra which are coordinated fully by $SiO_4$ tetrahedra in a condensed tectosilicate-like phase. This also suggests that the $Al^{[6]}$ and $Al^{[4]}$ species are in separate Al phases, and not bound within the same phyllosilicate-like phase. Structural determination can be made from both the observed $^{27}Al$ chemical shifts, and the $^{27}Al\{^{1}H\}$ REDOR dephasing behavior. The $^{27}Al$ chemical shift alone can be telling of the Al coordination environment. The $^{27}Al$ chemical shift varies significantly based on the first level Al coordination sphere and which allows peak assignments to $Al^{[6]}$ and $Al^{[4]}$ species based on their position. The second order coordination sphere also exhibits controls upon the $^{27}Al$ chemical shift. For $Al^{[6]}$ species the effect is only slight and differentiating between two $Al^{[6]}$ species like kaolinite and gibbsite is difficult based on chemical shift alone. In tectosilicates, the $Al^{[4]}$ chemical shift typically ranges between 55 and 68 ppm and represents $AlO_4$ tetrahedra which are directly bonded at all apices to $SiO_4$ tetrahedra. Phyllosilicates produce $Al^{[4]}$ peaks in the range of 70–80 ppm which result from the $AlO_4$ tetrahedron being bonded to an octahedral cation sheet and three $SiO_4$ tetrahedra (MacKenzie and Smith, 2002). For example, the beidellite sample produces a $Al^{[4]}$ peak with an peak maximum of 65.7 ppm and an isotropic chemical shift of 71.0 ppm (from $^{27}Al$ MQ/MAS) which are both outside the ranges observed for our samples.

Numerous empirical formulas have been developed which relate the chemical shift of $Al^{[4]}$ to structural features such as the average internuclear distance between tetrahedral sites, $d(T–T)$, (Kohn et al., 1997), and average Al–O–Si bond angle (Lippmaa et al., 1986; Phillips et al., 1989; Phillips and Kirkpatrick, 1994; Kohn et al., 1997). These studies were performed over a wide range of magnetic field strengths and assume peak maximum position ($\delta_{PM}$) represents the isotropic chemical shift. We acknowledge that second order quadrupole interactions do influence the position of the peak maximum, and our data from $^{27}Al$ MQ/MAS experiments indicate that the isotropic chemical shifts of the $Al^{[4]}$ peaks are slightly different from the positions of the peak maxima. However, we still use $\delta_{PM}$ in our calculations for the purposes of consistency with the prior studies. Using these models as first order approximations, we can begin to build an average structural model of $Al^{[4]}$ in the precipitated Al-phase. The uniformity of the $^{27}Al$ SP/MAS spectral characteristics indicate there is little variation in the local structure and that one structural model can be applied to all samples. Using the formula proposed by Kohn et al. (1997):

$$\delta_{PM} = -59.965 \cdot d(T-T) + 246.39 \quad (1)$$

and the chemical shifts in Table 4 we derive a range of $d(T–T)$ from 3.14 to 3.27 Å with an average distance of 3.22 Å. Using these same chemical shift values and the composite equation for Al–O–Si bond angle ($\alpha$) purposed in MacKenzie and Smith (2002):

$$\delta_{PM} = -0.532\alpha + 137 \quad (2)$$

we derive a range of Al–O–Si bond angles from 149° to 163° and an average of 157°. Using these values and assuming the average Si–O distance in the amorphous silica is equivalent to that of quartz, 1.61 Å, we obtain an average Al–O distance of 1.74 Å which agrees with that observed for $AlO_4$

Please cite this article in press as: Mason H. E., et al. The formation of metastable aluminosilicates in the Al–Si–$H_2O$ system: Results from solution chemistry and solid-state NMR spectroscopy. *Geochim. Cosmochim. Acta* (2011), doi:10.1016/j.gca.2011.07.031

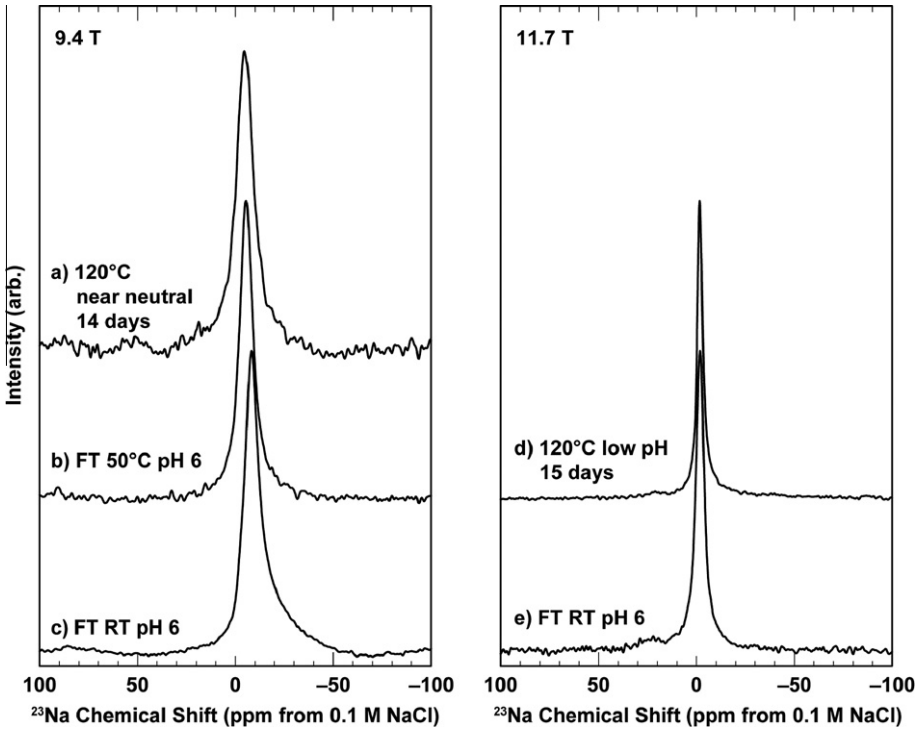


Fig. 9. Representative $^{23}$Na SP/MAS NMR spectra of three samples studied. (a) a sample made at near-neutral pH and 120 °C for a reaction period of 14 days, (b) the 50 °C sample made at pH 6.3, and (c) the 25 °C sample made at pH 6.3.

incorporated in biogenic silica (Gehlen et al., 2002). We must stress, however, that given the breadth of the lines observed in this study it is likely the above structural parameters represent average values, and that there exist a wide distribution of bond lengths and angles typifying an amorphous phase.

We can use the $^{27}$Al{$^{1}$H} REDOR data to investigate how Al is coordinated to the surrounding hydrated species ($OH^-$, $H_2O$, $H_3O^+$). Combining these results we propose a possible local structure for the $Al^{[6]}$ as presented in Fig. 10a. The dephasing behavior of the $Al^{[6]}$ species follow closely with that obtained for kaolinite (cf. Fig. 8a). The gibbsite curve produces a REDOR dephasing curve which trends at higher values than that of kaolinite. The Al–H distances in both these materials are reasonably comparable at 2.49 and 2.56 Å for gibbsite and kaolinite, respectively (Bish, 1993; Balan et al., 2006). The main difference in the REDOR dephasing likely arises from the abundance of H surrounding the Al octahedron. In gibbsite, Al is coordinated to six surrounding hydroxyls and in kaolinite it is only coordinated to three hydroxyl groups. While we cannot definitively assign the $Al^{[6]}$ peak in these experiments to kaolinite, we can state that it likely has a similar hydration environment.

We can also perform a similar analysis for the $Al^{[4]}$ species and one possibility for the average local structure envisioned is presented in Fig. 10b. The first important piece of information can be gleaned by considering the $^{27}$Al{$^{1}$H} REDOR results for mordenite and clinoptilolite. Both of these minerals have a substantial amount of $H_2O$ included within their structure. However, we observe only minor REDOR dephasing for mordenite, and almost none for clinoptilolite suggesting that the $H_2O$ in these minerals are not rigidly bound within the structure. We do observe significant amounts of dephasing for both analcime and beidellite where the $^{1}$H is present as rigidly bound $H_2O$ and hydroxyl groups, respectively. Since we observe large dephasing values for all $Al^{[4]}$ species we know that these species must be in association with rigidly bound $^{1}$H. Further, we can draw conclusions on their hydration environment by again investigating the structure of the two model minerals, analcime and beidellite, to which their dephasing behavior most closely aligns. In both cases, the exact location of the $^{1}$H in the structure is not well known so the Al–O distance to the hydrated species will be used as a proxy for the Al–H distance. As with many clay minerals, the exact crystal structure of beidellite is not known, but we will assume that on the local scale it is similar to that of montmorillonite. In the montmorillonite structure, the $Al^{[4]}$ is located proximal to a single hydroxyl at an average Al–O distance of 3.42 Å. The $Al^{[4]}$ in analcime is located at an average Al–O distance of 3.99 Å to a structural water molecule. Despite the shorter Al–O distance of beidellite it produces a REDOR curve exhibiting lower REDOR fractions than that for analcime. This again is due to the presence of more $^{1}$H in direct proximity to the Al in the analcime than in the beidellite. Given the similar dephasing behavior of the majority of the $Al^{[4]}$ peaks to that of analcime it is possible these $AlO_4$ tetrahedra are in close proximity (<4 Å) to structural $H_2O$. Another possibility is that the $AlO_4$ tetrahedra are still in close enough proximity to the abundant silanols in the amorphous silica substrate.

Please cite this article in press as: Mason H. E., et al. The formation of metastable aluminosilicates in the Al–Si–$H_2O$ system: Results from solution chemistry and solid-state NMR spectroscopy. *Geochim. Cosmochim. Acta* (2011), doi:10.1016/j.gca.2011.07.031

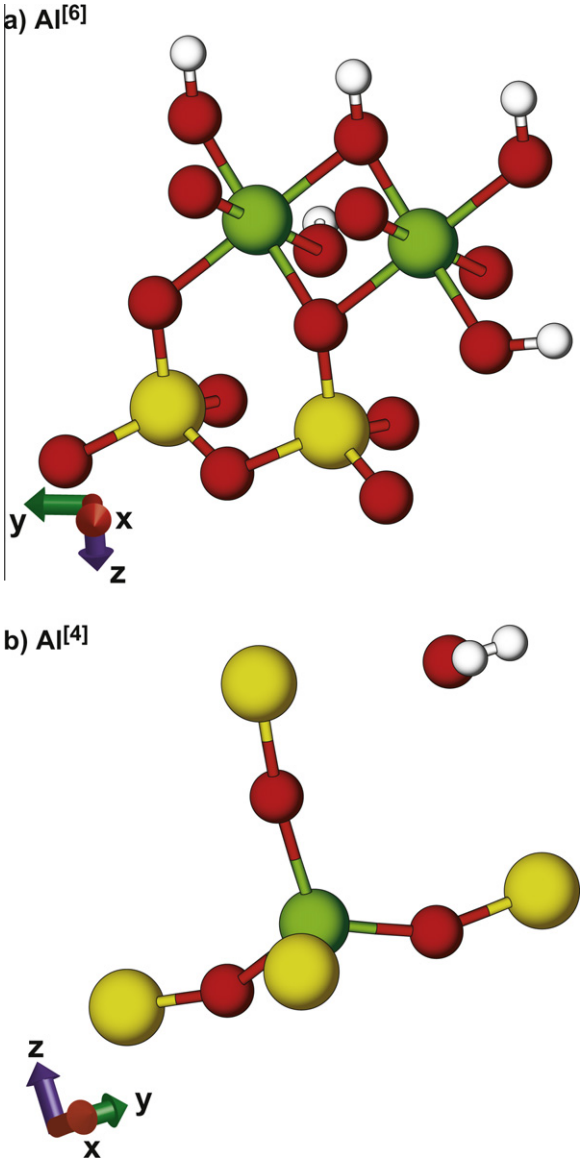


Fig. 10. Average local structural models derived from NMR data for the (a) $Al^{[6]}$ and (b) $Al^{[4]}$ phases. Green spheres represent Al, yellow spheres represent Si, red spheres represent O, and white spheres represent H. Positions are all approximate, and additional coordinating oxygens for the Si in the $Al^{[4]}$ model were omitted for simplicity. (For interpretation of the references to color in this figure legend, the reader is referred to the web version of this article.)

The trends we observe in the REDOR data do provide compelling evidence for the presence of structural $H_2O$, but we concede that we cannot definitively determine between these possibilities given the sparse REDOR curves collected for the uptake samples. However, the higher dephasing for the $Al^{[4]}$ in the 25 and 50 °C samples is likely due to the presence of higher amounts of structurally bound protons.

Given the results of the $^{23}Na$ NMR study we cannot conclusively state that Na is present in a charge balancing capacity. Nevertheless, Na could still serve this purpose in our system, but our current methods are unable to detect this fraction due to overwhelming signal arising from the surface sorbed species. If present, additional Na could exist as a structural constituent in the $Al^{[6]}$ phase, but it is more likely to serve as a charge balancing cation in the formation of the $Al^{[4]}$ phase.

Taken as a whole, these structural determinations can be used to build cohesive structural models. In both the $Al^{[6]}$ and $Al^{[4]}$ phases, the line widths preclude the presence of discrete crystalline Al-silicate phases. The hydration state suggests the $Al^{[6]}$ phase is kaolinite-like, and the $^{29}Si$ data indicates that at least in one case that allophane is present. The REDOR results for the $^{27}Al$ allophane peak also indicate a dephasing behavior similar to that of kaolinite. Given the similar chemical shift and large widths of the $Al^{[6]}$ peaks in these samples it may be possible to extend the allophane assignment to the other samples with the caveat that the peak is likely obscured in $^{29}Si$ spectra due to its relatively low abundance in these samples. One possibility for the $Al^{[4]}$ phase is a hydrated sodium aluminosilicate gel with a tectosilicate framework representing a metastable precursor to zeolitic phases such as analcime or even a hydrated albite. This could be especially relevant for the higher temperature experiments where such phases are more stable. The formation of such phase would certainly necessitate the incorporation of Na as a charge balancing cation. A second possibility is the Al is occluded within the amorphous silica. The $^{27}Al$ spectra for the $Al^{[4]}$ phases are broadly similar to those collected for Al incorporated as defects in opal (Brown et al., 2003; Paris et al., 2007). This particular substitution could be locally charged balanced through the co-location of silanol groups on neighboring silicate tetrahedra. However, with the given data we cannot confidently discriminate between these two possibilities.

### 4.2. Comparison to previous work on aluminum and silica

The results from this study allow us to draw some important conclusions about the interactions between Al and the amorphous silica surface. In this system, Al interacts to form metastable aluminosilicates, and the $Al^{[4]}$ and $Al^{[6]}$ are contained within separate phases. There is no evidence for the formation of $Al(OH)_3$ nor sorption of Al to the amorphous silica surface. These aluminosilicates form at micromolal concentrations, and the reactions here can be extended to marine diagenesis, geothermal systems, and carbon sequestration where similar dissolved Al concentrations have been observed (Gallup, 1997; Van Cappellen and Qiu, 1997a,b; Carroll et al., 1998, submitted for publication).

We can also use these results to update the model proposed by Houston et al. (2008) to include the formation of metastable aluminosilicate phases as the dominant active process. The previous model has suggested a multi-step process dependent on solution pH including $Al^{[4]}$ sorption, surface enhanced precipitation of $Al(OH)_3$, and the formation of amorphous $Al^{[4]}$-silicate. The Al concentrations in the current study are two to three orders of magnitude less than that of Houston et al. (2008), and provide a good test for sorption processes. The larger amount of $Al^{[4]}$ compared

Please cite this article in press as: Mason H. E., et al. The formation of metastable aluminosilicates in the Al–Si–$H_2O$ system: Results from solution chemistry and solid-state NMR spectroscopy. *Geochim. Cosmochim. Acta* (2011), doi:10.1016/j.gca.2011.07.031

to $Al^{[6]}$ in the higher pH experiments of Houston et al. (2008) likely result from higher Al and Si concentrations present in their batch experiments driving the formation of the $Al^{[4]}$ silicates.

The formation of metastable allophane-like aluminosilicate phases has been invoked as a possible controlling mechanism for Al solubility in surface waters (Doucet et al., 2001; Exley et al., 2002). The authors of these studies propose two phases which they term hydroxyl-aluminosilicate phases $HAS_A$ and $HAS_B$. They suggest that Al:Si is a critical control on their formation. $HAS_A$ is defined as an $Al^{[6]}$ dominant imogolite-like phase thought to form under conditions where $Al_{aq}$ is greater than $Si_{aq}$ and $HAS_B$ is an $Al^{[4]}$ dominant phase forming where $Al_{aq}$ is less than $Si_{aq}$. They conclude that $HAS_B$ is poorly hydrated, the $Al^{[4]}$ and $Al^{[6]}$ cohabitate within a single phase derived from $Al^{[4]}$ templating on the $HAS_A$ structure, and presumably that $Al^{[4]}$ charge balance is achieved through the presence of $Al^{[6]}$ octahedra. Our results instead show evidence that mutually exclusive hydrated $Al^{[4]}$ and $Al^{[6]}$ phases can form under conditions with very low Al:Si, and that Na could serve to charge balance the $Al^{[4]}$ silicate phase. It is possible, therefore, that the Al solubility could be controlled through a metastable-equilibrium between $Al^{[6]}$ and an $Al^{[4]}$ silicate phases similar to the following equations

$$Al_2Si_2O_5(OH)_4 + 2H^+ + Na^+ + SiO_2(aq) \leftrightarrow NaAlSi_3O_8 \cdot H_2O + Al^{3+} + 2H_2O \quad (3)$$

$$IAP = \{Al^{3+}\}/(\{H^+\}^2\{SiO_2(aq)\}) \quad (4)$$

rather than those based on the solubility of $HAS_B$ as proposed by Dobrzynski (2007). Such equations could be easily incorporated in models of Al and Si cycling.

There is abundant evidence in the literature that dissolved Al is concentrated in geothermal silica scales and accelerates the precipitation of amorphous silica (Gallup, 1997, 1998; Carroll et al., 1998). In the presence of dissolved silica, $Al(OH)_3$ has been shown to be unstable at 90 °C and it quickly forms both $Al^{[6]}$ and $Al^{[4]}$ silicate phases (Yokoyama et al., 2002). Based largely on those results, Yokoyama et al. (2002) and Nishida et al. (2009) proposed that the formation of $Al(OH)_3$ phases were necessary precursors to the formation of $Al^{[4]}$ phases in hydrothermal scales. The results of this current study suggest that these precursor phases may not be necessary, but more work is required to elucidate the mechanisms of aluminosilicate formation in these systems.

The findings of this study may also be relevant to geochemical alterations that occur when supercritical $CO_2$ is stored in deep saline aquifers to mitigate global warming (IPCC, 2007). Recent studies have shown that dissolution of iron-rich clays found in saline sandstone reservoirs drive the reactive chemistry in storage environments. Enhanced dissolution from high $CO_2$ solubility yields secondary precipitation of aluminum hydroxides or alumino-silicates (Carroll et al., submitted for publication). In these environments it is possible the dissolved Al and Si concentrations will be controlled the $Al^{[4]}$ and $Al^{[6]}$ silicate phases detected in this study.

## ACKNOWLEDGMENTS

We thank Victoria Genetti and Rachel Lindvall for collecting the ICP-MS data. We also thank two anonymous reviewers whose input led to many improvements in the manuscript. This work was funded by the Department of Energy, Office of Basic Energy Science and performed under the auspices of the U.S. Department of Energy by Lawrence Livermore National Laboratory under Contract W-7405-Eng-48 and Contract DE-AC52-07NA27344.

## REFERENCES

Alberti A., Davoli P. and Vezzalini G. (1986) The crystal structure refinement of a natural mordenite. *Z. Krisallogr.* **184**, 49–61.

Balan E., Lazzeri M., Morin G. and Mauri F. (2006) First-principles study of the OH-stretching modes of gibbsite. *Am. Mineral.* **91**, 115–119.

Barron P. F., Wilson M. A., Campbell A. S. and Frost R. A. (1982) Detection of imogolite in soils using solid state $^{29}Si$ NMR. *Nature* **299**, 616–618.

Betke C. M. and Yeakel S. (2010) *The Geochemists Workbench, Release 8.0, Hydrogeology Program*. Univ. Illinois, p. 308.

Bickmore B. R., Nagy K. L., Gray A. K. and Brinkerhoff A. R. (2006) The effect if $Al(OH)_4^-$ on the dissolution rate of quartz. *Geochim. Cosmochim. Acta* **70**, 290–305.

Blumenfeld A. L., Coster D. and Fripiat J. J. (1995) Brønsted acid sites and surface structure in zeolites: a high-resolution $^{29}Si$ NMR REDOR study. *J. Phys. Chem.* **99**, 15181–15191.

Blumenfeld A. L. and Fripiat J. J. (1997) $^{27}Al$–$^{1}H$ REDOR NMR and $^{27}Al$ spin–echo editing: a new way to characterize Brönsted and Lewis acidity in zeolites. *J. Phys. Chem. B* **101**, 6670–6675.

Brown L. D., Ray A. S. and Thomas P. S. (2003) $^{29}Si$ and $^{27}Al$ NMR study of amorphous and paracrystalline opals from Australia. *J. Non-Cryst. Solids* **332**, 242–248.

Bish D. L. (1993) Rietveld refinement of the kaolinite structure at 1.5K. *Clays Clay Min.* **41**, 738–744.

Carroll S. A., Maxwell R. S., Bourcier M. L., Martin S. and Hulsey S. (2002) Evaluation of silica–water surface chemistry using NMR spectroscopy. *Geochim. Cosmochim. Acta* **66**, 913–926.

Carroll S. A., McNab W. and Torres S. (submitted for publication) Experimental study of cement–sandstone/shale–brine–$CO_2$ interactions. *Geochem. Trans.*

Carroll S., Mroczek E., Alai M. and Ebert M. (1998) Amorphous silica precipitation (60 to 120 °C): comparison of laboratory and field rates. *Geochim. Cosmochim. Acta* **62**, 1379–1396.

Dixit S., Van Cappellen P. and van Bennekom A. J. (2001) Processes controlling solubility of biogenic silica and pore water build-up of silicic acid in marine sediments. *Mar. Chem.* **73**, 333–352.

Dobrzynski D. (2007) Chemistry of neutral and alkaline waters with low $Al^{3+}$ activity against hydroxylaluminosilicate $HAS_B$. The Evidence from ground and surface waters of the Sudetes Mts. (SW Poland). *Aquat. Geochem.* **13**, 197–210.

Doucet F. J., Schneider C., Bones S. J., Kretchmer A., Moss I., Tekely P. and Exley C. (2001) The formation of hydroxylaluminosilicates of geochemical and biological significance. *Geochim. Cosmochim. Acta* **65**, 2461–2467.

Exley C., Schneider C. and Doucet F. J. (2002) The reaction of aluminum with silicic acid solution: an important mechanism in controlling the biological availability of aluminum? *Coord. Chem. Rev.* **228**, 127–135.

Gallup D. L. (1997) Aluminum silicate scale formation and inhibition: scale characterization and laboratory experiments. *Geothermics* **26**, 483–499.

Gallup D. L. (1998) Aluminum silicate scale formation and inhibition (2): Scale solubilities and laboratory and field inhibition tests. *Geothermics* **27**, 485–501.

Gehlen M., Beck L., Calas G., Flank A. M., Van Bennekom A. J. and Van Buesekom J. E. E. (2002) Unraveling the atomic structure of biogenic silica: Evidence of the structural association of Al and Si in diatom frustules. *Geochim. Cosmochim. Acta* **66**, 1601–1609.

Gullion T. and Vega A. J. (2005) Measuring heteronuclear dipolar couplings for $I = 1/2$, $S > 1/2$ spin pairs by REDOR and REAPDOR NMR. *Prog. NMR Spectrosc.* **47**, 123–136.

Houston J. R., Herberg J. H., Maxwell R. S. and Carroll S. A. (2008) Association of dissolved aluminum with silica: connecting structure to surface reactivity using NMR. *Geochim. Cosmochim. Acta* **72**, 3326–3337.

Idlefonse P., Kirkpatrick R. J., Montez B., Calas G., Flank A. M. and Lagarde P. (1994) $^{27}$Al MAS NMR and aluminum X-ray absorption near edge structure study of imogolite and allophanes. *Clays Clay Min.* **42**, 276–287.

IPCC (2007) IPCC Fourth Assessment Report on Climate Change 2007: Synthesis Report. In *Prepared by Working Group I, II and III of the Intergovernmental Panel on Climate Change. Geneva, Switzerland* (eds. R. K. Pachauri and A. Reisinger).

Kim Y. and Kirkpatrick R. J. (1997) $^{23}$Na and $^{133}$Cs NMR study of cation adsorption on mineral surfaces: local environments, dynamics, and effects of mixed cations. *Geochim. Cosmochim. Acta* **61**, 5199–5208.

Kim Y. and Kirkpatrick R. J. (1998) High-temperature multinuclear NMR investigation of analcime. *Am. Mineral.* **83**, 339–347.

Kohn S. C., Henderson C. M. B. and Dupree R. (1997) Si–Al ordering in leucite group minerals and ion-exchanged analogues: an MAS NMR study. *Am. Mineral.* **82**, 1133–1140.

Lippmaa E., Samoson A. and Mägi M. (1986) High-resolution $^{27}$Al NMR of aluminosilicates. *J. Am. Chem. Soc.* **108**, 1730–1735.

MacKenzie K. J. D. and Smith M. E. (2002) *Multinuclear Solid-State NMR of Inorganic Materials*. Pergamon Press, Oxford.

Magi M., Lippmaa E., Samoson A., Engelhardt G. and Grimmer A. R. (1984) Solid-state high-resolution silicon-29 chemical shifts in silicates. *J. Phys. Chem.* **88**, 1518–1522.

Moroz N. K., Afanassyev I. S., Fursenko B. A. and Belitsky I. A. (1998) Ion mobility and dynamic disordering of water in analcime. *Phys. Chem. Miner.* **25**, 282–287.

Parfitt R. L. (2009) Allophane and imogolite: role in soil biogeochemical process. *Clay Miner.* **44**, 135–155.

Paris M., Fritsch E. and Reyes B. O. A. (2007) $^{1}$H, $^{29}$Si, and $^{27}$Al NMR study of the destabilization process of paracrystalline opal from Mexico. *J. Non-Cryst. Solids* **353**, 1650–1656.

Phillips B. L., Kirkpatrick R. J. and Putnis A. (1989) Si, Al ordering in leucite by high resolution $^{27}$Al MAS NMR-spectroscopy. *Am. Mineral.* **16**, 591–598.

Phillips B. L. and Kirkpatrick R. J. (1994) Short-range Si–Al order in leucite and analcime–determination of the configurational entropy from $^{27}$Al and variable-temperature $^{29}$Si NMR-spectroscopy of leucite, its Cs-exchanged and Rb-exchanged derivatives, and analcime. *Am. Mineral.* **79**, 1025–1031.

Nishida I., Shimida Y., Saito T., Okaue Y. and Yokoyama T. (2009) Effect of aluminum of the deposition of silica scales in cooling water systems. *J. Colloid Interface Sci.* **335**, 18–23.

Stone W. E. E., El Shafei G. M. S., Sanz J. and Selim S. A. (1993) Association of soluble aluminum ionic species with a silica-gel surface. A solid-state NMR study. *J. Phys. Chem.* **97**, 10127–10132.

Van Cappellen P. and Qiu L. (1997a) Biogenic silica dissolution in sediments of the Southern Ocean. I. Solubility. *Deep Sea Res. II* **44**, 1109–1128.

Van Cappellen P. and Qiu L. (1997b) Biogenic silica dissolution in sediments of the Southern Ocean. I. Kinetics. *Deep Sea Res. II* **44**, 1129–1149.

Van Cappellen P., Dixit S. and van Beusekom J. (2002) Biogenic silica dissolution in the oceans: Reconciling experimental and field-based dissolution rates. *Global Biogeochem. Cy.* **16**, 1075.

Vega A. J. (1992) MAS NMR spin locking of half-integer quadrupolar nuclei. *J. Magn. Reson.* **96**, 50–68.

Xue X. and Stebbins J. F. (1993) $^{23}$Na NMR chemical shifts and local Na coordination environments in silicate crystals, melts, and glasses. *Phys. Chem. Miner.* **20**, 297–307.

Yokoyama T., Taguchi S., Motomura Y., Watanabe K., Nakanishi T., Aramaki Y. and Izawa E. (2004) The effect if aluminum on the biodeposition of silica in hot spring water: chemical state of aluminum in siliceous deposits collected along the hot spring stream of Steep Cone hot spring in Yellowstone National Park, USA. *Chem. Geol.* **212**, 329–337.

Yokoyama T., Ueda A., Kato K., Mogi K. and Matsuo S. (2002) A study of the alumina–silica gel adsorbant for the removal of silicic acid from geothermal water: increase in adsorption capacity due to formation of amorphous aluminosilicate by adsorption of silicic acid. *J. Colloid Interface Sci.* **252**, 1–5.

*Associate editor:* William H. Casey

Please cite this article in press as: Mason H. E., et al. The formation of metastable aluminosilicates in the Al–Si–$H_2O$ system: Results from solution chemistry and solid-state NMR spectroscopy. *Geochim. Cosmochim. Acta* (2011), doi:10.1016/j.gca.2011.07.031